# Topological phases of a semi-Dirac Chern insulator in the presence of extended range hopping

Sayan Mondal and Saurabh Basu
*Department of Physics, Indian Institute of Technology Guwahati, Guwahati 781039, Assam, India*

(Received 4 April 2022; accepted 9 June 2022; published 29 June 2022)

We study the topological properties and the topological phase transitions therein of a semi-Dirac Haldane model on a honeycomb lattice in the presence of an extended range (third neighbor) hopping. While in the absence of third-neighbor hopping $t_3$ the system exhibits a gapless electronic spectrum, its presence creates an energy gap in the dispersion. However, the nature of the spectral gap, that is, whether it is trivial or topological, needs to be ascertained. We find that the answer depends on the value of $t_3$ and its interplay with the value of the on-site potential that breaks the sublattice symmetry, namely, the Semenoff mass $\Delta$. To elucidate our findings on the topological phases, we demonstrate two kinds of phase diagrams using the available parameter space, one in which the phases are shown in the $\Delta$-$t_3$ plane and one in a more familiar $\Delta$-$\phi$ plane ($\phi$ is the Haldane flux). The phase diagrams depict the presence of Chern insulating lobes comprising Chern numbers $\pm 2$ and $\pm 1$ for a certain range of values for $t_3$, along with trivial insulating regions (zero Chern number). Thus, there are phase transitions from one topological regime to another which are characterized by abrupt changes in the values of the Chern number. To support the existence of the topological phases, we compute counterpropagating chiral edge modes in a ribbon geometry. Finally, the anomalous Hall conductivity obtained by us shows plateaus at either $e^2/h$ or $2e^2/h$ corresponding to these topological phases.

DOI: 10.1103/PhysRevB.105.235441

## I. INTRODUCTION

In condensed-matter systems, whether a material possesses a topological phase has been of immense interest since the discovery of the quantum Hall effect (QHE) [1]. The QHE demonstrates that in the presence of a strong magnetic field, the Hall conductivity of a two-dimensional electron gas acquires a series of plateaus quantized in units of $e^2/h$. This quantization is due to the presence of discrete magnetic Bloch bands [2–7] or Landau levels [8–12] owing to the presence of a magnetic flux. The topological invariant that defines the quantization of the Hall conductivity, from a general perspective, is known as the Thouless-Kohmoto-Nightingale-Nijs invariant [2].

An external magnetic field initially appeared to be necessary to achieve QHE; however, Haldane proposed that even in the absence of an external magnetic flux, QHE can still be observed [13]. He introduced direction-dependent complex next-nearest-neighbor hopping in a honeycomb lattice, such as graphene, which breaks time reversal symmetry (TRS). This broken TRS is the only necessary criterion to observe QHE. The model proposed by Haldane is a two-band system, with the bands being characterized by a topological invariant known as the Chern number, and these quantized (integer) values of the Chern number yield a plateau in the Hall conductivity when the Fermi energy lies in the bulk gap. Further, a nonzero value of the Chern number and hence the quantized value of the Hall conductivity can be seen for a finite value of the phase $\phi$ (we shall call it Haldane flux) of the complex next-nearest-neighbor hopping. A nonzero value of the Semenoff mass $\Delta$, which breaks the sublattice symmetry in graphene, opens or closes a gap in the band structure [14]. The variation of the Semenoff mass with the Haldane flux presents a phase diagram that encodes opening and closing of the band gap alternately at the two Dirac points, which are usually called the **K** and **K**′ points [13,15].

In recent years, exploration of the topological properties associated with the Haldane model have progressed rapidly in quantum many-body systems [16–19] from both experimental and theoretical perspectives. Studies of two-dimensional Dirac systems have also been explored, such as Fe-based ferromagnetic insulators, $X\mathrm{Fe}_2(\mathrm{PO}_4)_2$, where $X$ may be Cs, K, La, etc. [20], in the Dice lattice [21], which hosts isotropic low-energy Dirac-like dispersions. However, certain other materials exist that display anisotropic dispersions at low energies, for example, quadratic along one direction in the Brillouin zone (BZ) and linear along the other one [22–24], which are known as semi-Dirac systems. Semi-Dirac dispersions have been found in a variety of materials, such as phosphorene under pressure and doping [25,26], electric fields [27,28], multilayered structures of $\mathrm{TiO}_2/\mathrm{VO}_2$ [29,30], quasi-two-dimensional organic conductor BEDT-$\mathrm{TTF}_2\mathrm{I}_3$ under pressure [31,32], oxidized silicene layer [33], deformed graphene [34], etc. Experimentally, semi-Dirac dispersions have been observed in layers of black phosphorene obtained via *in situ* doping of potassium atoms [35].

A natural question arises about whether semi-Dirac systems will show topological phases similar to those of their Dirac counterpart. To gain insight into the answer to this question, we explore whether and how the lowering of symmetry induced by anisotropic dispersion modifies the topological properties of the system. However, to achieve a topological

 

phase, we need to break the TRS of the system, either by including a perpendicular magnetic field or via adding the complex second-neighbor hopping (the Haldane term). Here, we choose the latter option. However, unlike in the Dirac case, the addition of the complex second-neighbor hopping in the semi-Dirac system does not open a gap in the electronic spectrum, and hence, the system remains a semimetal, with the conduction and valence bands touching each other at a point intermediate to the **K** and **K**′ points in the BZ (the **M** point). A little introspection reveals that, in such a scenario, we can add a real third-neighbor hopping to open up a gap in the energy spectrum and hence look for the existence of the topological phases. A semi-Dirac system with the Haldane term has been discussed in the literature [36]. However, we are not aware of studies of the semi-Dirac system with the Haldane term and a real third-neighbor hopping. An important dividend of such an exercise will be accessing regions in the phase diagram with large values of the Chern number [37], which also facilitates studying the topological phase transitions between phases with different Chern numbers.

Theoretically, certain systems have been predicted that show nontrivial topological phases with higher values of Chern numbers, such as a star lattice (decorated honeycomb structure) [38], where the Chern number $|C| = 3$, along with $|C| = 1$ and $|C| = 2$, has been observed. Also a third-neighbor hopping has been added in the multiorbital triangular lattice [39], which shows higher Chern numbers. Further, in a spin-orbit coupled system, along with the presence of a staggered flux in a honeycomb lattice [40,41], it is found that the spin Chern numbers and the total Chern numbers are nonzero, where the values may either be high or low depending on the values of the parameters used. In the case of an ultracold atomic gas on a triangular lattice [42,43], such higher Chern numbers have also been observed in the presence of the spin-orbit coupling. In classical systems, multiple higher Chern numbers, for example, $C = 1, 2, 3, 4$, have been observed in an acoustic Chern insulator, such as a sonic crystal [44]. Higher values of Chern numbers have also been predicted in magnetic doped topological insulators [45] and Cr-doped thin laminar sheets of $Bi_2(Se, Te)_3$ [46]. On the experimental front, higher Chern numbers have been realized in $MnBi_2Te_4$ at high temperature [47,48], multilayer structures of magnetically doped and undoped topological insulators [49], etc.

Motivated by the above scenario, here, we discuss the topological properties of a semi-Dirac system in the presence of third-neighbor (between different sublattices) hopping. We shall show that inclusion of the third-neighbor hopping shifts the band minima from the boundary towards the interior of the BZ and makes the system a Chern insulator, with Chern numbers of $\pm 2$ for certain values of the hopping amplitude. The addition of the Semenoff mass to the problem changes the Chern number from $\pm 2$ to $\mp 1$. Consequently, we obtain the plateaus of the Hall conductivity, which are quantized as $Ce^2/h$, with $C$ being the Chern number, and acquire values $\pm 1$ and $\pm 2$.

This paper is organized as follows: In Sec. II we show the semi-Dirac Hamiltonian in the presence of a Haldane term and real third-neighbor hopping on a honeycomb lattice. In Sec. III, we investigate the topological properties by computing the Chern number for various values of the amplitude of the third-neighbor hopping and obtain phase diagrams that demonstrate the existence (or absence) of the nontrivial topological phases. In Sec. IV, we study the structure of the edge modes in a nanoribbon for various relevant values of the second- and third-neighbor hopping amplitudes. Hence, we compute the anomalous Hall conductivities, which exhibit plateaus quantized in units of $e^2/h$, in Sec. V and finally conclude with a brief summary of our results in Sec. VI.

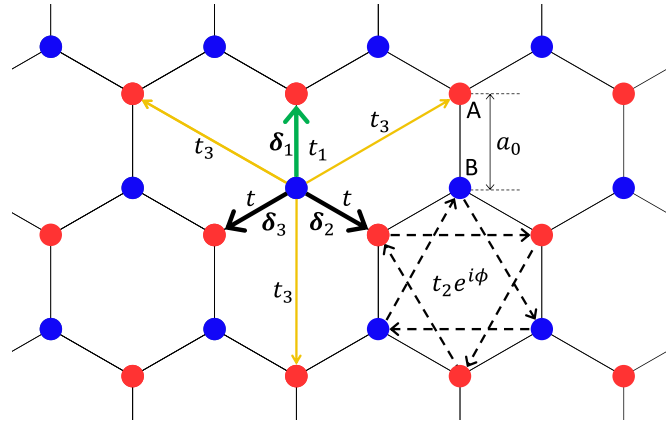


FIG. 1. A honeycomb lattice is shown, where the red and the blue circles represent sublattices A and B, respectively. In the $\boldsymbol{\delta}_2$ and $\boldsymbol{\delta}_3$ directions the N2 hopping strengths are the same ($t$), while in the $\boldsymbol{\delta}_1$ direction it is $t_1$. The N3 hopping is shown by the yellow arrows.

## II. MODEL HAMILTONIAN

We consider a tight-binding Hamiltonian on a honeycomb lattice with hopping between the various neighbors, which can be written as

$$H = -\sum_{\langle i,j\rangle} t_{ij} c_i^\dagger c_j + t_2 \sum_{\langle\langle i,j\rangle\rangle} e^{i\phi_{ij}} c_i^\dagger c_j + t_3 \sum_{\langle\langle\langle i,j\rangle\rangle\rangle} c_i^\dagger c_j + \sum_i \Delta_i c_i^\dagger c_i + \text{H.c.} \tag{1}$$

The first term is the nearest-neighbor (N1) hopping. The N1 hopping strengths along the $\boldsymbol{\delta}_2$ and $\boldsymbol{\delta}_3$ directions are $t$, while in the third direction, that is along $\boldsymbol{\delta}_1$, the strength is $t_1$, as shown in Fig. 1. The N1 vectors are given by $\boldsymbol{\delta}_1 = a_0(0, 1)$, $\boldsymbol{\delta}_2 = a_0(\sqrt{3}/2, -1/2)$, and $\boldsymbol{\delta}_3 = a_0(-\sqrt{3}/2, -1/2)$. In the first term, $t_{ij} = t_1$ or $t$ when $j$ connects the neighbors $\boldsymbol{\delta}_1$ or $\boldsymbol{\delta}_{2,3}$ that belong to the other sublattice, respectively. We have assumed two different values of $t_1$, such as $t_1 = t$ and $t_1 = 2t$. The value $t_1 = t$ represents the well-known isotropic Dirac case, graphene, while $t_1 = 2t$ denotes the semi-Dirac case and is the focus of this work. The second term is the Haldane term comprising a complex second-neighbor (N2) hopping with an amplitude $t_2$ and a complex phase denoted by $\phi_{ij}$, where $\phi$ assumes positive (negative) values if the electron hops in the clockwise (counterclockwise) direction. The third term represents the third-neighbor (N3) hopping between different sublattices, and the fourth term represents the on-site energy (Semenoff mass), which assumes values of $+\Delta$ and $-\Delta$ for sublattices A and B, respectively. Performing a Fourier transform of Eq. (1), we can write the Hamiltonian in momentum

space as

$$H(\mathbf{k}) = h_x(\mathbf{k})\sigma_x + h_y(\mathbf{k})\sigma_y + h_z(\mathbf{k})\sigma_z + h_0(\mathbf{k})I = \mathbf{h}(\mathbf{k})\cdot\boldsymbol{\sigma} + h_0(\mathbf{k})I, \quad (2)$$

where

$$h_x(\mathbf{k}) = \left\{t_1\cos k_y + 2t\cos\frac{k_y}{2}\cos\frac{\sqrt{3}k_x}{2}\right\} + t_3\{\cos 2k_y + 2\cos k_y\cos\sqrt{3}k_x\}, \quad (3)$$

$$h_y(\mathbf{k}) = \left\{-t_1\sin k_y + 2t\sin\frac{k_y}{2}\cos\frac{\sqrt{3}k_x}{2}\right\} + t_3\{\sin 2k_y - 2\sin k_y\cos\sqrt{3}k_x\}, \quad (4)$$

$$h_z(\mathbf{k}) = \Delta - 2t_2\sin\phi\left\{2\sin\frac{\sqrt{3}k_x}{2}\cos\frac{3k_y}{2} - \sin\sqrt{3}k_x\right\}, \quad (5)$$

and

$$h_0(\mathbf{k}) = 2t_2\cos\phi\left\{2\cos\frac{\sqrt{3}k_x}{2}\cos\frac{3k_y}{2} + \cos\sqrt{3}k_x\right\}, \quad (6)$$

where $\sigma_i$ ($i \in x, y, z$) denote the $2\times 2$ spin-1/2 Pauli matrices which represent the sublattice degrees of freedom and $I$ is the $2\times 2$ identity matrix. The energy dispersion can be obtained as

$$E(\mathbf{k}) = h_0(\mathbf{k}) \pm \sqrt{h_x(\mathbf{k})^2 + h_y(\mathbf{k})^2 + h_z(\mathbf{k})^2}, \quad (7)$$

where the $+$ and $-$ signs refer to the upper (conduction) band and the lower (valence) band, respectively. In the absence of $t_2$ and $t_3$, the band dispersion is linear along one direction and quadratic along its perpendicular direction [50] about the band touching **M** point in the BZ. We refer to this as the zero mode in our subsequent discussion.

Now, if we add a small N3 hopping, namely, $t_3$, then the zero modes shift from the **M** point towards the interior of the BZ, as shown in Figs. 2(b)–2(d). There are four zero modes inside the first BZ for a nonzero value of $t_3$. Let us call these points where the zero modes occur **Λ** points. For example, one of the zero modes for a particular value of $t_3$, namely, $t_3 = t$, occurs approximately at a particular **Λ** point, namely, $\mathbf{\Lambda}_1 = (\frac{1.1560\pi}{3\sqrt{3}a_0}, \frac{1.5487\pi}{3a_0})$, while that for a different value of $t_3$, namely, $t_3 = 3t$, approximately occurs at another **Λ** point, $\mathbf{\Lambda}_2 = (\frac{1.0805\pi}{3\sqrt{3}a_0}, \frac{1.2403\pi}{3a_0})$. For other values of $t_3$, namely, $t_3 > 3t$, the zero modes remain fixed at the same locations as that for $t_3 = 3t$.

Now, if we turn on the N2 hopping, $t_2$ then the spectral gaps open up at these Λ points in the BZ where the zero modes occur, and hence, the system behaves as an insulator. However, in the absence of $t_3$ (with $t_2$ being nonzero), there is no gap at the **M** point, and the dispersion is anisotropic linear (linear along both directions, but with different velocities along the $x$ and $y$ directions) about the **M** point, which makes the system a semimetal, as discussed in Ref. [36]. In Figs. 2(e) and 2(f), we show the band structures for the semi-Dirac system in the absence and in the presence of $t_2$, respectively, for nonzero values of $t_3$. In our calculations, we have fixed the values of the Haldane flux $\phi$, N1 hopping $t_1$, and the Semenoff mass $\Delta$ to $\pi/2$, $2t$, and zero, respectively. The corresponding band structures for the Dirac system were discussed in Refs. [51,52], and we skip them here to make our discussion concise.

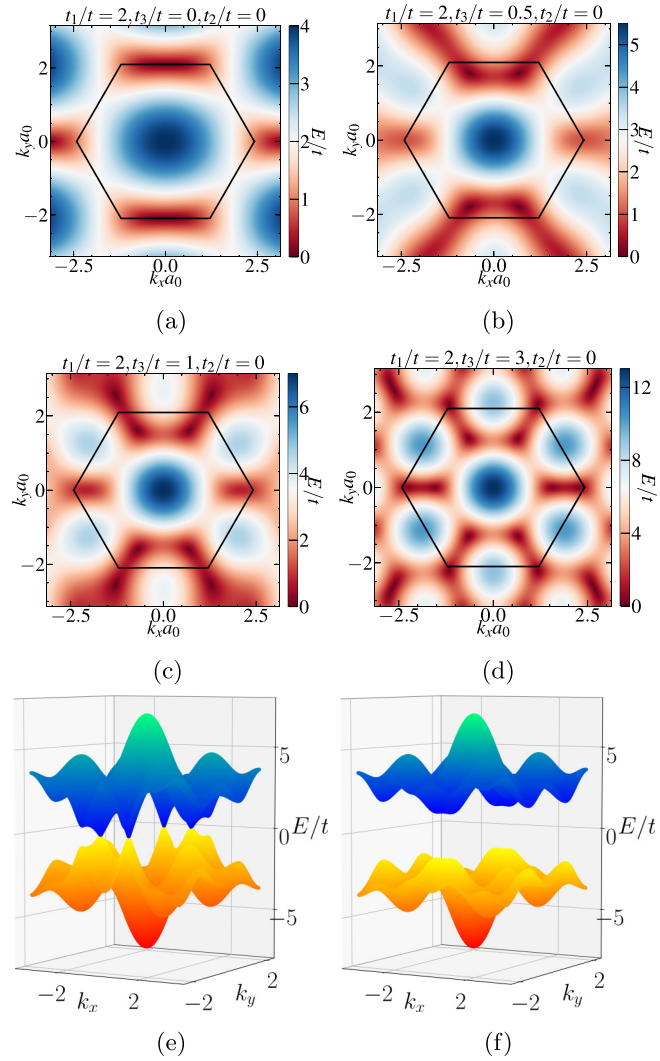


FIG. 2. The top view of the band structure of the semi-Dirac ($t_1 = 2t$) system is depicted for (a) $t_3/t = 0$, (b) $t_3/t = 0.5$, (c) $t_3/t = 1$, and (d) $t_3/t = 3$. The hexagons in each plot represent the first Brillouin zone. In the calculations, we have fixed $t_2 = 0$ and $\Delta = 0$. (e) and (f) Three-dimensional depictions of the band structure for the semi-Dirac system for $t_2 = 0$ and $t_2 = 0.5t$, respectively, where we have used $\Delta = 0$ and $\phi = \pi/2$.

It may be noted that $t_3$ is indeed a parameter and the values used may not have experimental relevance. The reason is that the value of the real second-neighbor hopping is of the order of 0.1 eV [53], which would mean that $t_3$ is even smaller. However, the phase diagrams presented in Sec. III demand the value of $t_3$ to be of the order of $t$ or even larger in order to access topological phases with different Chern numbers.

## III. THE PHASE DIAGRAM

In this section we obtain the phase diagram by numerically calculating the Chern number of the system. Since in this

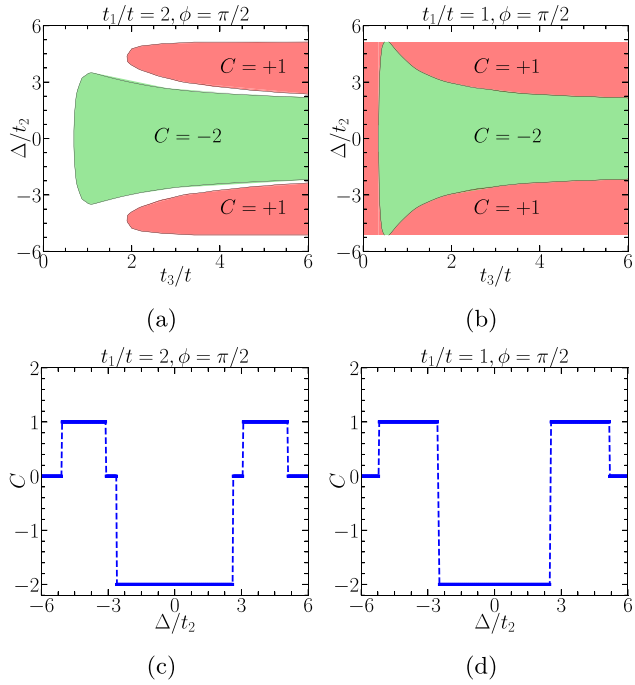


FIG. 3. The Chern number of the lower band is depicted as a function of $\Delta$ and $t_3$ for (a) $t_1/t = 2$ and (b) $t_1/t = 1$. The colored regions signify the Chern insulating regions with nonzero Chern numbers ($C = +1$ for the red region and $C = -2$ for the green one), while the white region denotes the trivial insulating phase with $C = 0$. We show the variation of $C$ as a function of $\Delta$ for a particular value of $t_3$, say, $t_3 = 3t$, for (c) $t_1/t = 2$ and (d) $t_1/t = 1$. In this calculation, the Haldane flux $\phi$ is kept fixed at $\pi/2$. The topological phase transitions are implied via $C$ discontinuously changing values between $1 \to 0 \to -2$.

model the complex N2 hopping term breaks the TRS, nonzero values and hence nontrivial phases with a finite Chern number are expected. The inversion symmetry breaking on-site energies $\pm\Delta$ on different sublattices opens or closes energy gaps in the energy spectrum at the $\Lambda$ points. We compute the Chern number via [54,55]

$$C = \frac{1}{2\pi} \iint_{\mathrm{BZ}} \Omega(k_x, k_y) dk_x dk_y, \tag{8}$$

where $\Omega(k)$ denotes the $z$ component of the Berry curvature [56], which is given by

$$\Omega(k_x, k_y) = \frac{\mathbf{h}}{2|\mathbf{h}|^3} \cdot \left( \frac{\partial \mathbf{h}}{\partial k_x} \times \frac{\partial \mathbf{h}}{\partial k_y} \right), \tag{9}$$

where $\mathbf{h}(\mathbf{k})$ is defined in Eq. (1). It should be noted that in the absence of an N3 hopping, the Chern number is always zero for any arbitrary value of $\Delta$ and $\phi$ for the semi-Dirac case ($t_1 = 2t$), even though the time reversal symmetry remains broken. However, in the presence of the nonzero N3 hopping, we may obtain nonzero values for the Chern number. In Fig. 3(a) we depict the Chern number corresponding to the lower band as a function of $\Delta$ and $t_3$ for Haldane flux $\phi = \pi/2$. As can be seen in Fig. 3(a), there are two regions denoted in red and green. The region in red indicates the value of the Chern number is $C = 1$, while the green region indicates $C = -2$. In addition, there is also a finite region denoted in white which corresponds to a trivial region with $C = 0$. In the absence of $t_3$ or at small values of $t_3$, namely, $t_3 < 0.68t$, for all values of $\Delta$, the trivial region prevails. We observe the topological phase with Chern number $C = -2$ beyond a certain value of the N3 hopping $t_3$, namely, $t_3 \gtrsim 0.68t$, for zero Semenoff mass ($\Delta = 0$). If we increase the value of $\Delta$, then we observe the $C = -2$ phase for a range of values of $t_3$, such as $0.68t \lesssim t_3 \lesssim 1.9t$. However, for $t_3 \gtrsim 1.9t$, there are two topological phases with Chern numbers $C = 1$ and $C = -2$, which depend on the value of $\Delta$. For example, for $t_3 = 3t$, a phase transition occurs from the $C = 0$ to $C = 1$ phase at $\Delta \simeq -5.04t_2$. $C$ again drops to zero at $\Delta \simeq -3.11t_2$. Beyond $\Delta \simeq -2.56t_2$ the Chern number becomes $-2$ and remains $-2$ until $\Delta \simeq 2.56t_2$, when the Chern number vanishes again. The Chern number becomes 1 at $\Delta \simeq 3.11t_2$ and finally vanishes again for $\Delta \gtrsim 5.04t_2$. Thus, a series of phase transitions occurs at $t_3 = 3t$. There is always a trivial region (with $C = 0$) between the two Chern insulating regions with two different Chern numbers (the white region between the red and green regions). Further, as one increases the value of $t_3$, vanishing Chern numbers are obtained for lower values of $\Delta$. As a result, the width of the Chern insulating region with $C = -2$ (the green region) shrinks with the increase of $t_3$, or equivalently, we can say that the width of the $C = 1$ region increases with the increase in $t_3$. The trivial region [shown in white in Fig. 3(a)] gets narrower as one increases the value of $t_3$.

This phenomenon is somewhat different in the Dirac case [see Fig. 3(b)], where we can see a nonzero Chern number (namely, $C = 1$) even in the absence of the N3 hopping, that is, the Haldane model. The phase persists for very small values of $t_3$. However, in the presence of N3 hopping, we obtain a phase with Chern number $C = -2$ or $C = 1$ depending on the value of $\Delta$. Further, unlike the semi-Dirac case, there is no trivial regime in between the two different Chern insulating regimes, that is, the red and green regions. If we fix the value of $t_3$, say, $t_3 = 3t$, and calculate the Chern numbers for increasing values of $\Delta$, then we observe the Chern number jump from $C = -2$ to $C = 1$ at $\Delta \simeq 2.55t_2$. Finally, the Chern number drops to zero from a value of $C = 1$ at $\Delta = 3\sqrt{3}t_2$. The values of $\Delta$ at which the Chern number changes from a value of $C = -2$ to $C = 1$ depend on the value of the N3 hopping $t_3$ [see the shoulderlike region in Fig. 3(b)]. However, the values of $\Delta$ at which the Chern number vanishes from a value of $C = 1$ does not depend upon $t_3$. It should be noted that the calculations are done for a Haldane flux $\phi = \pi/2$. If we change $\phi$ to $-\pi/2$, then the phase diagram will remain identical, except that the Chern numbers will undergo a sign change.

In Figs. 3(c) and 3(d) we show the variation of the Chern number as a function of $\Delta$ for the semi-Dirac ($t_1 = 2t$) and Dirac ($t_1 = t$) systems, respectively, for a particular value of $t_3$, say, $t_3 = 3t$. As can be seen for the semi-Dirac case [see Fig. 3(c)], there are phase transitions occurring from $C = 0$ to $C = 1$ and then again to $C = 0$ as one increases $\Delta$. With a further increase of $\Delta$, $C$ drops to $-2$. To quote some numerical values, the plateau at $C = -2$ exists for a range of $\Delta$, that is, $-2.56t_2 \lesssim \Delta \lesssim 2.56t_2$. With a further increase in the value of $\Delta$, $C$ drops to zero and then rises again to 1 and finally

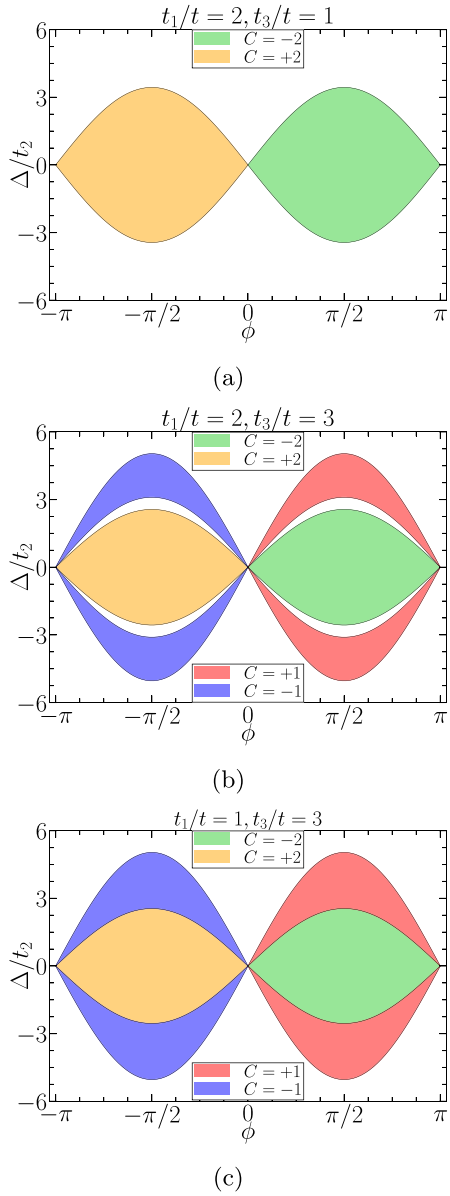


FIG. 4. The Chern numbers of the lower band are shown as a function of $\Delta$ and $\phi$ for (a) $t_1/t = 2$ and $t_3/t = 1$, (b) $t_1/t = 2$ and $t_3/t = 3$, and (c) $t_1/t = 1$ and $t_3/t = 3$. In each plot, the green and the orange regions denote the Chern insulating phase with Chern numbers of $-2$ and $+2$, respectively, while the red and the blue regions imply Chern numbers of $+1$ and $-1$, respectively. Further, the white region denotes the trivial topological regime with zero Chern number.

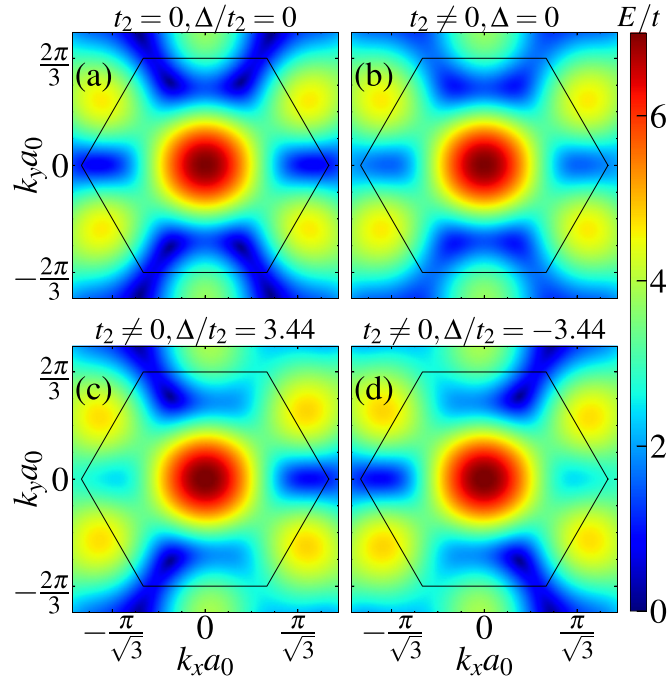


FIG. 5. The conduction band of the semi-Dirac system ($t_1 = 2t$) is shown in (a) in the absence of $t_2$ and the Semenoff mass $\Delta$, while the same in the presence of a nonzero $t_2$ is presented in (b)–(d) for $\Delta = 0$, $\Delta/t_2 = 3.44$, and $\Delta/t_2 = -3.44$, respectively. The values of $t_3$ and $\phi$ are taken as $t$ and $\pi/2$, respectively.

vanishes. The plateaus at $C = 1$ persist for some values of $\Delta$, such that, $-5.04t_2 \lesssim \Delta \lesssim -3.11t_2$ and $3.11t_2 \lesssim \Delta \lesssim 5.04t_2$. Similar phase transitions are observed for the Dirac case [see Fig. 3(d)], except that there are direct phase transitions from $C = 1$ to $C = -2$ or vice versa. The $C = -2$ plateau occurs for $-2.55t_2 < \Delta < 2.55t_2$, while the plateaus at $C = 1$ occur for $-3\sqrt{3}t_2 \leqslant \Delta \lesssim -2.55t_2$ and $2.55t_2 \lesssim \Delta \leqslant 3\sqrt{3}t_2$.

Figure 4 shows the phase diagram in the $\Delta$-$\phi$ plane corresponding to the lower band for both the semi-Dirac and Dirac cases. For both of them, the values of the Chern number depend on the value of the N3 hopping amplitude (see Fig. 3).

In Fig. 4(a), we show the phase diagram for the semi-Dirac case for $t_3 = t$. As can be seen, there are two Chern insulating regions with Chern numbers $C = -2$ (green region) and $C = +2$ (yellow region). The phase diagram is similar to that of the Haldane model, except that the values for the Chern number are different in this case. Further, the widths of the Chern insulating lobes are smaller than those in the Haldane model. Now, if we increase the value of $t_3$ (say, $t_3 = 3t$), we shall see additional Chern insulating regions emerge, with the Chern numbers given by $C = +1$ (red region) and $C = -1$ (blue region), as depicted in Fig. 4(b). A trivial insulating phase with $C = 0$ exists between the two Chern insulating regions, that is, between the green and red regions or between the yellow and blue regions. These types of phase diagrams are in complete contrast to the Dirac case, where the trivial insulating phase is absent, as shown in Fig. 4(c). The width of the Chern insulating region with $C = -2$ is greater in the Dirac case than in the semi-Dirac case [see Fig. 4(c)], as is evident from the $\Delta$-$t_3$ phase diagram [Fig. 3(b)]. For $t_3$ to be vanishingly small, we note that the phase diagram becomes similar to that of the Haldane model.

The reason to have a value of the Chern number of $|C| = 2$ is that we have multiple zero modes in the presence of $t_3$ (and in the absence of $t_2$) inside the first BZ for the semi-Dirac system. For example, when $t_3 = t$, the zero modes occur at four $\Lambda$ points, as depicted in Fig. 5(a), which are perceptible from the dark blue color. Gaps open up at those $\Lambda$ points, as we turn on the N2 hopping $t_2$ [see Fig. 5(b)]. The Chern number of the system becomes $-2$. Now, if we keep increasing the value of the Semenoff mass $\Delta$, the gaps at two out of the four $\Lambda$ points decrease and, finally, vanish at $\Delta \approx 3.4372$ [see

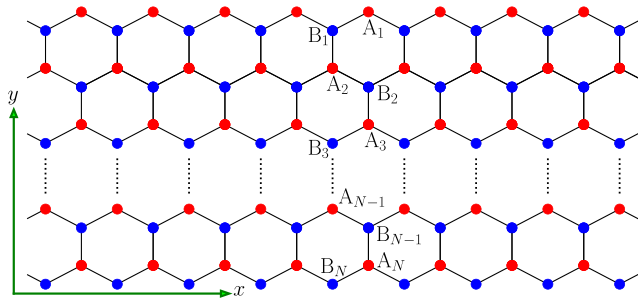


FIG. 6. Schematic diagram of the ribbon. The edge current flows along the zigzag edges ($x$ axis) of the ribbon.

Fig. 5(c)], where a topological phase transition takes place. For $\Delta \gtrsim 3.4372$, the gaps open up again; however, the Chern number vanishes. A similar gap-closing scenario occurs at the remaining two $\Lambda$ points for $\Delta \approx -3.4372$ [see Fig. 5(d)].

The phase diagrams presented in Figs. 3 and 4 aid us in identifying specific values of $t_3$ and $\Delta$ to explore the nature of the topological phases. We achieve that via the numerical computation of the edge states and the anomalous Hall conductivity, as discussed below. These quantities are investigated for $t_3 = 0.5t$, $t$, and $3t$, where we have considered $\Delta = 0$ corresponding to $t_3 = 0.5t$ and $t$, while the $t_3 = 3t$ case has been studied for $\Delta = 0$ and $\Delta = 4t_2$, which correspond to $C = -2$ and $C = 1$, respectively.

## IV. EDGE STATES

In order to understand whether the nature of the band gaps is topological or trivial, we look for the existence (or absence) of the edge states. To achieve this, we consider the system to have semi-infinite ribbon geometry. Such a scenario breaks the periodicity along a particular direction, while the translational symmetry is preserved along the perpendicular direction. We take the semi-infinite ribbon [57,58] to be finite along the $y$ direction and infinite along the $x$ direction. We further label the sites along the $y$ direction as $A_1$, $B_1$, $A_2$, $B_2$, ... $A_N$, $B_N$, etc., as shown in Fig. 6. Since the translational invariance is preserved along the $x$ direction, we can Fourier transform the operators along only the $x$ direction, that is, use $c^{\dagger}_{x,y} = \sum_k e^{ikx} c^{\dagger}_{k,y}$. This yields two sets of coupled eigenvalue equations for the wave functions which can be written as

$$E_k a_{k,n} = -[t\{1 + e^{(-1)^n ik}\} b_{k,n} + t_1 b_{k,n-1}] - 2t_2 \left[\cos(k+\phi) a_{k,n} + e^{(-1)^n \frac{ik}{2}} \cos\left(\frac{k}{2} - \phi\right)\{a_{k,n-1} + a_{k,n+1}\}\right] + t_3[b_{k,n+3} + 2b_{k,n-1}\cos k] + \Delta a_{k,n}, \tag{10}$$

$$E_k b_{k,n} = -[t\{1 + e^{(-1)^{n+1} ik}\} a_{k,n} + t_1 a_{k,n+1}] - 2t_2 \left[\cos(k-\phi) b_{k,n} + e^{(-1)^{n+1} \frac{ik}{2}} \cos\left(\frac{k}{2} + \phi\right)\{a_{k,n-1} + a_{k,n+1}\}\right] + t_3[a_{k,n-3} + 2a_{k,n+1}\cos k] - \Delta b_{k,n}, \tag{11}$$

where $n$ denotes the site index. $n$ assumes integer values in the range $[1 : N]$, with $N$ being the total number of unit cells along the $y$ direction. In Eqs. (10) and (11), $a_{k,n}$ and $b_{k,n}$ are the coefficients of the wave functions corresponding to the $n$th A and B sublattices, respectively. Here, $k$ is the momentum along the periodic $x$ direction, which is rendered dimensionless by defining $k = \sqrt{3}a_0 k_x$. The width $D$ of the ribbon along the $y$ direction is related to $N$ via $D(N) = a_0(\frac{3N}{2} - 1)$. In our work, we use $N = 128$, and hence, the ribbon has a width of $191a_0$. By solving Eqs. (10) and (11) one can get the band structure of the nanoribbon, as shown in Fig. 7 for a fixed value of the Haldane flux, namely, $\phi = \pi/2$. As can be seen, one of the edge modes from the lower band crosses over to the upper band as a function of $k_x$, and another one crosses over in the opposite direction. These edge modes are responsible for a finite value of the Hall conductivity, provided the Fermi energy lies in the bulk gap. In Fig. 7(a), we show the edge states for the semi-Dirac ($t_1 = 2t$) system corresponding to a particular value of the N3 hopping, for example, $t_3 = t$. The red dashed line represents the Fermi energy $E_F$, and the points where the edge modes intersect the Fermi energy are shown by green dots. The edge currents corresponding to points $p$ and $r$ flow along one of the zigzag edges of the ribbon, and the edge currents corresponding to points $p$ and $s$ travel along the other edge [see Fig. 7(g)]. However, their flows are in opposite directions since the velocity of the electron is proportional to $\partial E/\partial k$, which changes sign at $(q, s)$ compared to those at $(p, r)$.

Owing to the presence of a pair of edge states, there will be finite Hall conductivity with a plateau occurring at a value of $2e^2/h$, with the factor of 2 denoting the number of edge modes [59]. This result is consistent with the Chern number phase diagram [see Fig. 3(a)], where the Chern number is found to have a value of $-2$ for $t_3 = t$ and $\Delta = 0$. In contrast, we get a single edge mode, along either edge of the ribbon, for $t_3 = 3t$ and $\Delta = 4t_2$, as shown in Fig. 7(f). In this case, we show the edge currents corresponding to points $q$ and $r$ in Fig. 7(h). This result is also consistent with the phase diagram [Fig. 3(b)], where we find $C = 1$. For $t_2 = 0.5$ and $\Delta = 0$, the edge modes are shown in Fig. 7(c). It is clearly visible that the edge modes have split from the bulk. Thus, one can say that the edge modes do not contribute to the edge current and hence the system possesses zero Hall conductivity.

The edge states for the Dirac system ($t_1 = t$) are shown for comparison in Figs. 7(d), 7(e), and 7(f). The plots show the presence of a single edge mode at points $p$ and $s$ for $t_3 = 0.1t$ and $\Delta = 0$ [Fig. 7(d)], which propagates at two opposite edges of the ribbon corresponding to points $p$ and $s$. Such a situation yields a plateau in the Hall conductivity at $e^2/h$. This result is similar to that of the Haldane model. Now, if we increase the value of the N3 hopping $t_3$ to, say, $t_3 = t$ [Fig. 7(e)], a pair of edge modes appears, and they

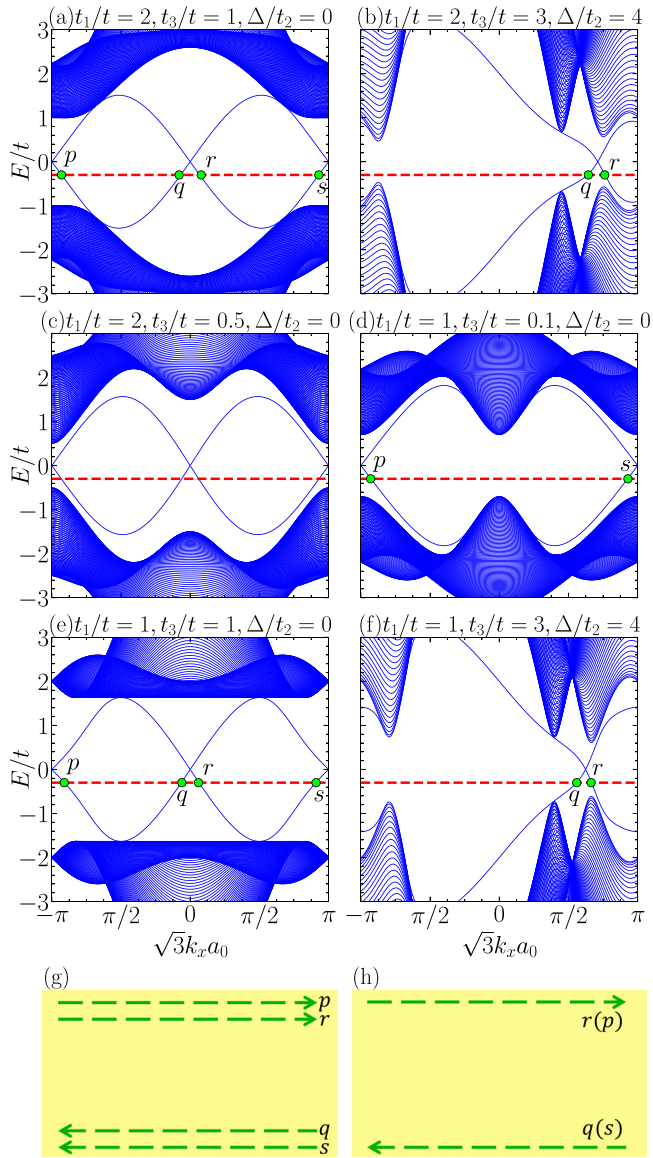


FIG. 7. The energy spectra of the ribbon as a function of the dimensionless momentum $k$ (here, $k$ denotes $\sqrt{3}a_0k_x$) for the semi-Dirac system ($t_1/t = 2$) are shown for (a) $t_3/t = 2$, $\Delta/t_2 = 0$, (b) $t_3/t = 3$, $\Delta/t_2 = 4$, and (c) $t_3/t = 0.5$, $\Delta/t_2 = 0$, while for the Dirac system ($t_1/t = 1$) they are shown for (d) $t_3/t = 0.1$, $\Delta = 0$, (e) $t_3/t = 1$, $\Delta = 0$, and (f) $t_3/t = 3$, $\Delta/t_2 = 4$. The green dots in each plot signify the intersection of the edge states with the Fermi energy $E_F$ (shown via the red dashed line). (g) and (h) denote schematic diagrams of a part of the ribbon. The arrows in (g) represent the edge currents corresponding to the points in (a) and (e), while in (h) the edge currents are shown corresponding to the points in (b), (d), and (f).

propagate along two different edges of the ribbon; however, these two pairs are counterpropagating at the opposite edges [see Fig. 7(h)]. In this case, the Hall plateau will be quantized in units of $2e^2/h$. The pair of edge currents will be there as long as the Semenoff mass $\Delta$ remains at a zero value. However, as we introduce a finite value of $\Delta$, there is a possibility that there will be a single edge mode at each edge, as depicted in Fig. 7(f). Here, we see that the edge modes are along either

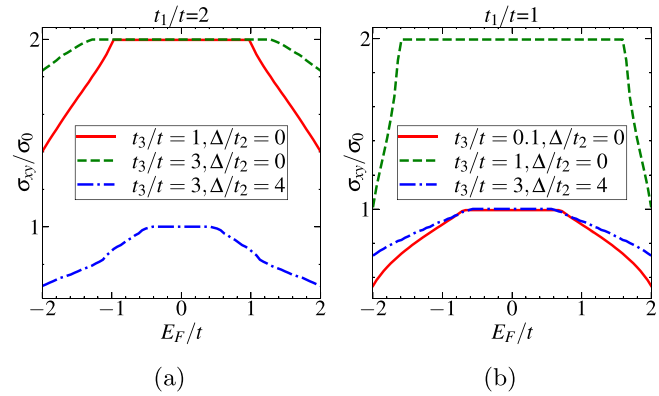


FIG. 8. The variation of anomalous Hall conductivity $\sigma_{xy}$ is shown as a function of the Fermi energy $E_F$ for (a) $t_1/t = 2$ and (b) $t_1/t = 1$. Here, $\sigma_0 = e^2/h$ is the unit of the Hall conductivity. In this calculation we have fixed the N2 hopping $t_2$ at $0.5t$ and the Haldane flux $\phi$ at $\pi/2$.

edge of the ribbon corresponding to points $q$ and $r$, as shown in Fig. 7(h). The number of edge currents along either edge of the ribbon is consistent with their values for the Chern numbers, namely, $C = 1$ and $C = -2$ [see Fig. 3(b)].

## V. ANOMALOUS HALL CONDUCTIVITY

The anomalous Hall conductivity requires a nonzero local Berry curvature. In order to calculate the Hall conductivity, we first obtain the Berry curvature of the system using Eq. (9) and then use the following formula [60–62]:

$$\sigma_{xy} = \frac{\sigma_0}{2\pi} \sum_{\lambda} \int \frac{dk_x dk_y}{(2\pi)^2} f\left(E^{\lambda}_{k_x,k_y}\right) \Omega(k_x, k_y), \qquad (12)$$

where $E^{\lambda}(k_x, k_y)$ denotes the electronic energies and $\lambda = +1$ and $-1$ represent the upper and the lower bands, respectively. $\sigma_0 (= e^2/h)$ sets the scale for $\sigma_{xy}$. $f(E) = [1 + e^{(E-E_F)/K_BT}]^{-1}$ is the Fermi-Dirac distribution function, with $E_F$ being the Fermi energy and $T$ being the absolute temperature. Using Eqs. (9) and (12), the Hall conductivity is calculated numerically at zero temperature ($T = 0$) as a function of $E_F$ and is shown in Fig. 8(a) for the semi-Dirac system ($t_1 = 2t$). We see that as long the Fermi energy lies in the gapped region, the Hall conductivity shows a plateau quantized in units of $2e^2/h$ for $t_3 = t$ and $\Delta = 0$. Since the integral is performed over the occupied states for a given value of $E_F$, the Hall conductivity decreases as $E_F$ moves away from the gapped region, that is, towards the bulk. If we consider the Semenoff mass $\Delta$ to be zero, we see that the plateaus occur at $2e^2/h$, as shown by the green and red curves in Fig. 8(a). However, in the presence of a finite value of $\Delta$, there is a possibility of getting a plateau at $e^2/h$ in $\sigma_{xy}$, as shown by the blue curve in Fig. 8(b). These results are supported by the respective values for the Chern numbers. Thus, for $C = -2$, we get the Hall plateau quantized at a value $2e^2/h$, and for $C = 1$, we find it is quantized at $e^2/h$.

To make a comparison with the Dirac case, that is, for $t_1 = t$, we show the anomalous Hall conductivity in Fig. 8(b). As can be seen, with a small N3 hopping (say, $t_3 = 0.1t$), the Hall plateau is quantized in units of $e^2/h$ [the red curve in Fig. 8(b)]. If we increase the value of the N3 hopping,

the quantized Hall conductivity is seen at $2e^2/h$. Now, if we add the Semenoff mass term, the quantized Hall conductivity acquires a plateau at $e^2/h$. The value of $\Delta$ up to which the $e^2/h$ plateau is retained depends on the value of $t_3$. In Fig. 8(b), we show the Hall conductivity for a nonzero $\Delta$ with the blue curve corresponding to $t_3 = 3t$. The existence of the $e^2/h$ Hall plateau is noted for a certain range of $\Delta$, that is, $2.5t_2 \lesssim \Delta \lesssim 3\sqrt{3}t_2$, corresponding to a fixed value of N3 hopping, namely, $t_3 = 3t$. Similar to the case for the semi-Dirac system, the quantized Hall conductivity of the Dirac system is fully consistent with the corresponding Chern number phase diagrams [see Fig. 3(b)].

## VI. CONCLUSION

We have shown that, in the semi-Dirac system, adding a third-neighbor hopping causes the zero modes to move inward into the BZ from the boundary. The addition of the Haldane term creates spectral gaps at those points. We have obtained two different phase diagrams, namely, in the parameter spaces defined by $\Delta$-$\phi$ and $\Delta$-$t_3$ after computing the Chern numbers. The $\Delta$-$t_3$ phase diagram for the semi-Dirac case shows a different scenario than the Dirac case in the following sense. There is always a trivial regime between the two Chern insulating regimes ($C = -2$ and $C = 1$), which is absent for the Dirac case. The $\Delta$-$\phi$ phase diagram for the semi-Dirac case shows that one may have Chern insulating regions with either $|C| = 2$ and $|C| = 1$ or only $|C| = 2$, depending on the value of the N3 hopping $t_3$. The computation of the edge states shows additional crossing of the edge modes corresponding to $|C| = 2$. Finally, the anomalous Hall conductivities for several values of $t_3$ demonstrate the existence of Hall plateaus quantized either at $2e^2/h$ or at $e^2/h$ depending on the values of their Chern number.


[1] K. von Klitzing, Rev. Mod. Phys. **58**, 519 (1986).
[2] D. J. Thouless, M. Kohmoto, M. P. Nightingale, and M. den Nijs, Phys. Rev. Lett. **49**, 405 (1982).
[3] D. J. Thouless, Phys. Rev. B **27**, 6083 (1983).
[4] J. E. Avron, R. Seiler, and B. Simon, Phys. Rev. Lett. **51**, 51 (1983).
[5] M. Kohmoto, Ann. Phys. (Berlin, Ger.) **160**, 343 (1985).
[6] Q. Niu, D. J. Thouless, and Y.-S. Wu, Phys. Rev. B **31**, 3372 (1985).
[7] *The Quantum Hall Effect*, edited by R. E. Prange and S. M. Girvin (Springer, Berlin, 1990).
[8] R. B. Laughlin, Phys. Rev. B **23**, 5632(R) (1981).
[9] S. A. Trugman, Phys. Rev. B **27**, 7539 (1983).
[10] S. Ilani, J. Martin, E. Teitelbaum, J. H. Smet, D. Mahalu, V. Umansky, and A. Yacoby, Nature (London) **427**, 328 (2004).
[11] P. Vasilopoulos, Phys. Rev. B **32**, 771 (1985).
[12] D. Tong, arXiv:1606.06687.
[13] F. D. M. Haldane, Phys. Rev. Lett. **61**, 2015 (1988).
[14] G. W. Semenoff, Phys. Rev. Lett. **53**, 2449 (1984).
[15] T. Thonhauser and D. Vanderbilt, Phys. Rev. B **74**, 235111 (2006).
[16] M. Z. Hasan and C. L. Kane, Rev. Mod. Phys. **82**, 3045 (2010).
[17] Y. Ando, J. Phys. Soc. Jpn. **82**, 102001 (2013).
[18] X.-L. Qi and S.-C. Zhang, Rev. Mod. Phys. **83**, 1057 (2011).
[19] J. E. Moore, Nature (London) **464**, 194 (2010).
[20] H. S. Kim and H. Y. Kee, npj Quant Mater **2**, 20 (2017).
[21] B. Dey, P. Kapri, O. Pal, and T. K. Ghosh, Phys. Rev. B **101**, 235406 (2020).
[22] P. Dietl, F. Piéchon, and G. Montambaux, Phys. Rev. Lett. **100**, 236405 (2008).
[23] S. Banerjee, R. R. P. Singh, V. Pardo, and W. E. Pickett, Phys. Rev. Lett. **103**, 016402 (2009).
[24] K. Ziegler and A. Sinner, Europhys. Lett. **119**, 27001 (2017).
[25] A. S. Rodin, A. Carvalho, and A. H. Castro Neto, Phys. Rev. Lett. **112**, 176801 (2014).
[26] J. Guan, Z. Zhu, and D. Tománek, Phys. Rev. Lett. **113**, 046804 (2014).
[27] A. N. Rudenko, S. Yuan, and M. I. Katsnelson, Phys. Rev. B **92**, 085419 (2015).
[28] C. Dutreix, E. A. Stepanov, and M. I. Katsnelson, Phys. Rev. B **93**, 241404(R) (2016).
[29] V. Pardo and W. E. Pickett, Phys. Rev. Lett. **102**, 166803 (2009).
[30] V. Pardo and W. E. Pickett, Phys. Rev. B **81**, 035111 (2010).
[31] Y. Suzumura, T. Morinari, and F. Piéchon, J. Phys. Soc. Jpn. **82**, 023708 (2013).
[32] Y. Hasegawa, R. Konno, H. Nakano, and M. Kohmoto, Phys. Rev. B **74**, 033413 (2006).
[33] C. Zhong, Y. Chen, Y. Xie, Y.-Y. Sun, and S. Zhang, Phys. Chem. Chem. Phys. **19**, 3820 (2017).
[34] G. Montambaux, F. Piéchon, J.-N. Fuchs, and M. O. Goerbig, Phys. Rev. B **80**, 153412 (2009).
[35] J. Kim, S. S. Baik, S. H. Ryu, Y. Sohn, S. Park, B.-G. Park, J. Denlinger, Y. Yi, H. J. Choi, and K. S. Kim, Science **349**, 723 (2015).
[36] S. Mondal, P. Kapri, B. Dey, T. K. Ghosh, and S. Basu, J. Phys.: Condens. Matter **33**, 225504 (2021).
[37] S. Saha, T. Nag, and S. Mandal, Phys. Rev. B **103**, 235154 (2021).
[38] W.-C. Chen, R. Liu, Y.-F. Wang, and C.-D. Gong, Phys. Rev. B **86**, 085311 (2012).
[39] S. Yang, Z.-C. Gu, K. Sun, and S. Das Sarma, Phys. Rev. B **86**, 241112(R) (2012).
[40] Y. Yang, Y. F. Zhang, L. Sheng, and D. Y. Xing, Europhys. Lett. **105**, 27005 (2014).
[41] Y. Yang, X. Li, and D. Xing, Eur. Phys. J. B **89**, 217 (2016).
[42] A. Alase and D. L. Feder, Phys. Rev. A **103**, 053305 (2021).
[43] M. Łącki, J. Zarkrzewski, and N. Goldman, SciPost Phys. **10**, 112 (2021).
[44] H. Zhao, T. Zhang, X. Zhang, M.-H. Lu, and Y.-F. Chen, Front. Phys. **10**, 844417 (2022).
[45] C. Fang, M. J. Gilbert, and B. A. Bernevig, Phys. Rev. Lett. **112**, 046801 (2014).

[46] J. Wang, B. Lian, H. Zhang, Y. Xu, and S.-C. Zhang, Phys. Rev. Lett. **111**, 136801 (2013).
[47] J. Ge, Y. Liu, J. Li, H. Li, T. Luo, Y. Wu, Y. Xu, and J. Wang, Natl. Sci. Rev. **7**, 1280 (2020).
[48] W. Zhu, C. Song, H. Bai, L. Liao, and F. Pan, Phys. Rev. B **105**, 155122 (2022).
[49] Y. F. Zhao, R. Zhang, R. Mei, L. Zhou, H. Yi, Y. Q. Zhang, J. Yu, R. Xiao, K. Wang, N. Samarth, M. H. W. Chan, C. X. Liu, and C. Z. Chang, Nature (London) **588**, 419 (2020).
[50] P. Sinha, S. Murakami, and S. Basu, Phys. Rev. B **102**, 085416 (2020).
[51] D. Sticlet and F. Piéchon, Phys. Rev. B **87**, 115402 (2013).
[52] C. Bena and L. Simon, Phys. Rev. B **83**, 115404 (2011).
[53] A. H. Castro Neto, F. Guinea, N. M. R. Peres, K. S. Novoselov, and A. K. Geim, Rev. Mod. Phys. **81**, 109 (2009).
[54] D. J. Thouless, *Topological Quantum Numbers in Nonrelativistic Physics* (World Scientific, Singapore, 1998).
[55] J. E. Avron, L. Sadun, J. Segert, and B. Simon, Phys. Rev. Lett. **61**, 1329 (1988).
[56] C.-X. Liu, S.-C. Zhang, and X.-L. Qi, Annu. Rev. Condens. Matter Phys. **7**, 301 (2016).
[57] K. Nakada, M. Fujita, G. Dresselhaus, and M. S. Dresselhaus, Phys. Rev. B **54**, 17954 (1996).
[58] D. Sticlet, F. Piéchon, J.-N. Fuchs, P. Kalugin, and P. Simon, Phys. Rev. B **85**, 165456 (2012).
[59] Y. Hatsugai, Phys. Rev. B **48**, 11851 (1993).
[60] D. Xiao, M.-C. Chang, and Q. Niu, Rev. Mod. Phys. **82**, 1959 (2010).
[61] D. Culcer, A. MacDonald, and Q. Niu, Phys. Rev. B **68**, 045327 (2003).
[62] K. Saha, Phys. Rev. B **94**, 081103(R) (2016).